

Article

# Identification of the most potent bioactive natural compound as main protease inhibitor of SARS-CoV-2: Molecular docking, molecular dynamics simulations and MM-PBSA studies

Sana Begum<sup>1</sup>, Vishal K. Singh<sup>2</sup>, Priyanka Kumari<sup>1</sup>, Anup Som<sup>1</sup>

<sup>1</sup>Centre of Bioinformatics, Institute of Interdisciplinary Studies, University of Allahabad, Prayagraj - 211002, India

<sup>2</sup>Department of Chemistry, Institute of Science, Banaras Hindu University, Varanasi - 221005, India

The first three authors contributed equally

E-mail: som.anup@gmail.com

Received 22 July 2024; Accepted 31 August 2024; Published online 15 September 2024; Published 1 December 2024



## Abstract

Emergence of COVID-19 and thereafter intensive research on bioactive natural compounds against SARS-CoV-2, identified a large number of phytochemicals (i.e., plants-derived) and mycochemicals (i.e., fungi-derived) as potential inhibitors with proven antiviral properties against SARS-CoV-2, but there are no comparative study on the reported compounds. A comparative study among the previously identified/reported main protease (Mpro) inhibitors of SARS-CoV-2 can lead to the most potent compound that eventually helps to make an effective drug lead against SARS-CoV-2. Through manual literature curation, we selected 57 potential bioactive compounds and screened them against Mpro protein of SARS-CoV-2. A series of *in silico* screening such as binding affinity, drug-like properties, pharmacokinetic, physicochemical, and ADMET studies identified top ten compounds as potential Mpro inhibitors. Further, docking studies prioritized the top two compounds namely Norquinadoline A and Quinadoline B, based on their predicted affinity for the target protein. Binding free energy calculations further emphasized them as top candidates for effective Mpro inhibitors that hold promise for drug development against COVID-19. In-depth molecular dynamics studies and MM/PBSA analysis culminated in the recognition of Norquinadoline A as the most potent Mpro inhibitor of SARS-CoV-2. Thus, Norquinadoline A can be used as lead compound in further drug discovery process after *in vitro* and *in vivo* experimental studies.

**Keywords** COVID-19; SARS-CoV-2; main protease; phytochemicals; mycochemicals; molecular docking; drug-likeness; toxicity; MD simulations; MM-PBSA analyses.

Network Biology  
ISSN 2220-8879  
URL: <http://www.iaees.org/publications/journals/nb/online-version.asp>  
RSS: <http://www.iaees.org/publications/journals/nb/rss.xml>  
E-mail: [networkbiology@iaees.org](mailto:networkbiology@iaees.org)  
Editor-in-Chief: WenJun Zhang  
Publisher: International Academy of Ecology and Environmental Sciences

## 1 Introduction

COVID-19, a highly transmissible, severe respiratory human disease caused by the novel coronavirus

SARS-CoV-2 rendered devastation in the entire world and has been declared as a global pandemic by the World Health Organization (<https://covid19.who.int/>). It first emerged in late 2019 in China and then spread to nearly all the continents. Though, it exhibits approximately ~2 to 4% fatality rate, lower than the other members of same family (SARS-CoV-1 ~10% fatality rate; MERS-CoV ~37% fatality rate), it is more contagious, resulting in higher overall death rates (Abdelghany et al. 2021; Rubio et al. 2021).

SARS-CoV-2 is an enveloped RNA virus belonging to the *Coronaviridae* family and genus *beta coronavirus* (Gorbalenya et al. 2020; Som et al. 2022). The genome has a variable number of open reading frames (around 6 to 11). Viral RNA located in the ORF1 translates two polyproteins and encodes 16 non-structural proteins (NSP), while the remaining ORF codes for structural proteins (V'kovski et al. 2021; Singh et al. 2022a). Coronavirus has four major structural proteins, namely the Spike (S) protein, envelope (E) protein, membrane (M) protein, and nucleocapsid (N) protein (Singh et al. 2021; Sharma et al. 2021). One of the main druggable targets of SARS-CoV-2 is main protease (Mpro) because it is essential for the life cycle of SARS-CoV-2. It cleaves the overlapping pp1a and pp1ab polyproteins which are needed for SARS-CoV-2 replication and transcription (Yadav et al. 2021; Bhardwaj et al. 2021).

Extensive research was carried out and subsequently identified potential targets for drug development against Coronaviruses (CoVs), highlighting the Angiotensin-converting enzyme II (ACE2) entry receptor, the Mpro, and the RNA-dependent RNA polymerase (RdRp). However, drugs designed for the ACE2 entry receptor and the RdRp have exhibited significant side effects and reduced efficacy (Singh et al., 2021). In contrast, Mpro emerges as a promising and well-characterized drug target within the CoV family. The absence of homologs of Mpro with similar cleavage in human make it attractive target, which, showed less adverse effect as compare to other targets.

The Mpro plays a pivotal role in the life cycle of SARS-CoV-2 by processing polyproteins generated during viral RNA transcription. This critical enzyme targets and cleaves up to 11 sites on a large replicase protein (1ab, ~790 kDa), and inhibiting Mpro effectively halts viral replication. Importantly, the absence of known human homologs with identical cleavage specificity minimizes the potential for adverse toxic outcome. The amino acid sequences of Mpro in SARS-like coronaviruses exhibit remarkable conservation across various species, underscoring its significance in viral function. Mpro typically forms a dimer, consisting of protomers A and B, with three distinct domains regulating its structure and function. Domains I and II forming an antiparallel b-barrel structure, these domains span residues 8–101 (Domain I) and 102–184 (Domain II) house the substrate-binding pocket, essential for the catalytic activity of Mpro. Domain III spans residues 201–303 and forms an antiparallel globular cluster with five  $\alpha$ -helices (Fig. 1). Crucial for regulating protomer dimerization through a salt-bridge interaction, further stabilizing the overall structure of Mpro. Dimerization of Mpro is vital for its catalytic activity, particularly in shaping the S1 pocket of the catalytic site. This occurs through the interaction of N-terminal residues (N-finger) of each protomer with Glu166 of the other protomer. In SARS-CoV-2 Mpro, the dimer features a contact interface primarily between domain II of protomer A and the N-finger residues of protomer B, closely resembling the structural features observed in SARS-CoV. An intriguing mutation, (SARS-CoV-2) 285A, in SARS-CoV-2 Mpro has led to the closer alignment of domains III of different protomers. This mutation results in a slightly increased catalytic efficiency compared to SARS-CoV, attributed to changes in enzyme dynamics that transmit the mutation's effects to the catalytic center (Dai et al. 2020).

Drug discovery for the very infectious COVID-19 is a challenging job owing to frequent mutations and generation of new variants. Also, the drug shouldn't have severe side effects. Thus, bioactive natural compounds came into the consideration to expedite the work of finding effective drugs against COVID-19 using bioinformatics and computational tools. The use of *in-silico* approaches has demonstrated their critical

role in acceleration of drug discovery efforts in the various studies (Hossain et al. 2023; Nag et al. 2021). Moreover, the costs of synthesis in case of synthesized compounds are cut down in case of phytochemicals and mycochemicals. Accordingly, a large number of researches works on phytochemical compounds have been carried out. One such work by Majnooni and co-workers presented candidate phytochemicals with protective effect in lung injury which is the main COVID-19 complication (Majnooni et al. 2020). Besides phytochemicals, marine fungus-derived compounds also play a vital source for developing new drugs with greater efficacy and specificity for therapeutics and represent a promising source of unique chemical structures for the drug discovery (Belachew et al. 2021). Also, these sources have the advantage of large-scale production of the compounds with low-cost effect.

Natural products showed a several biological activities including anticancer, antibacterial, antiviral, and antioxidant etc. Several review articles have been published both on phytochemicals and mycochemicals like alkaloids, steroids, diterpenoid lactones, aliphatic, and glycosides with reported antiviral effects as SARS-CoV-2 therapeutics (Banerjee et al. 2021; Bhardwaj et al. 2021; Patel et al. 2021; Swain et al. 2021; Tam et al. 2021). Similarly, the phytochemicals derived from individual plants (Shanmugarajan et al. 2020; Chikhale et al. 2021) and exotic medicinal phytochemicals indigenous to particular geographical areas (Barlow et al. 2012; Hostettmann et al. 2000; Lu et al. 2022; Ogunyemi et al. 2020) had been reported against SARS-CoV-2. Likewise, Indian geography is also a rich source of biodiversity with more than 7000 plant species used as medicinal plants compounds had been explored to target SARS-CoV-2 proteins (Nallusamy et al. 2021; Roshni et al. 2022).

Overall, intensive research on phytochemical and mycochemical compounds against SARS-CoV-2 identified/reported a large number of compounds as potential inhibitors with profound antiviral properties against SARS-CoV-2, but there are no comparative studies on the identified/reported phytochemical/mycochemical compounds. A comparative study of the potential inhibitors can lead to the most potent compound that eventually helps to make an effective drug lead against SARS-CoV-2. Based on the above observation, this work focuses on compiling all the reported potential phytochemical and mycochemical compounds to derive a dataset of ligand libraries of bioactive compounds with proven antiviral activity to screen against Mpro target protein using computational approaches. Through meticulous literature curation, we prepared a ligand library of 57 potential compounds and screened them against Mpro protein of SARS-CoV-2. A series of *in silico* screening such as binding affinity, drug-like properties, pharmacokinetic, physicochemical, and ADMET studies identified the top ten compounds as potential Mpro inhibitors. Additionally, the top two compounds were chosen for docking studies, reaffirming the precision of AutoDock Vina in generating native-like dock poses. Subsequently, a refinement process was implemented, rearranging the top two compounds based on their docking scores. This strategic approach aimed to enhance the selection process for further simulations, ensuring a more focused and informed investigation. Further, the simulation study (complex stability) and energetics study (binding interactions stability) illustrated Norquinadoline A (**compound 1**) and Quinadoline B (**compound 2**) as the most potent inhibitors for Mpro protein.

## 2 Method

### 2.1 Ligand library preparation

A library of 57 previously reported key Mpro inhibitors was selected through a literature search from reputed publications based on proven antiviral activity against SARS CoV-2 (listed in supplementary Table S1). These 57 prominent compounds include alkaloids, flavones, terpenoids, and phenolic compounds which have been observed to combat viral infections and also reported as potential Mpro inhibitors of SARS-COV-2. Their 3D structures were retrieved from the PubChem database (<https://pubchem.ncbi.nlm.nih.gov/>) in SDF format and

converted to PDBQT format using Open Babel (<http://openbabel.org>), and prepared in an acceptable format for docking to Autodock vina (<https://vina.scripps.edu/>).

## 2.2 Protein preparation

The 3D crystal structure of SARS-CoV-2 in complex (PDB ID: 5R80 (Douangamath et al.2020), resolution: 1.93 Å) was retrieved from the RCSB protein data bank (<https://www.rcsb.org/>). The AutoDock Tool (<https://autodock.scripps.edu/>) docking preparation tool was used to prepare the protein for docking and was saved as pdbqt format that contains hydrogen atoms in all polar residuals, removes water and adds Kollman's charge.

## 2.3 Pharmacokinetic studies

Phytochemical/mycochemical compounds have been designed as possible antiviral agents using *in-silico* structure-based approaches. SwissADME software (<http://www.swissadme.ch/>) was used to predict the physicochemical properties and pharmaceutically relevant properties of compounds. Assessment of properties was done using a thumb rule, i.e., Lipinski's rule of five to find out the drug-like characteristics of the molecules, and molecules violating more than one rule were rejected for further studies (Lipinski et al. 2004; Ghosh et al. 2020a; Singh et al. 2022a).

## 2.4 Drug-likeness properties

Online software Molinspiration (<https://www.molinspiration.com/>) was used to predict the macromolecular targets for designed molecules. The bioactivity scores were evaluated to analyze some more drug-like properties such as solubility, permeability, metabolic stability and transporter effects.

## 2.5 *In silico* physicochemical and ADMET studies

ADMET properties affect pharmacological activity of drug candidates (Khushboo et al. 2024). ADMET properties prediction (viz. aqueous solubility [log S], skin permeability [log Kp], synthetic accessibility score, absorption, distribution, metabolism, excretion, and toxicity) of the 57 natural compounds were calculated by using pkCSM-Biosig (<https://biosig.lab.uq.edu.au/pkcsm/>) and Swiss ADME (<http://www.swissadme.ch/>) software (Daina et al., 2017).

## 2.6 Virtual screening

Virtual screening was carried out to screen the prepared library of natural compounds towards the Mpro binding site using AutoDock Vina (<https://vina.scripps.edu/>). Autodock Tool was used for preparing the receptor. This includes removing water and heteroatoms, adding polar hydrogen only, adding Kollman charge, and repairing missing atoms. For each compound, the number of docked conformation (modes) was set to 20, the number of runs (exhaustiveness) was 100 and the energy was set to 4. The center of the grid box was set to X: 10.9010, Y: 1.4615, Z: 18.287, and the dimensions (Å) were X: 60, Y: 60, Z: 60. BIOVIA Discovery Studio 2021 (<https://discover.3ds.com/discovery-studio-visualizer-download>) was used to study interactions between the docked complexes. The lowest docking score (in kcal/mol) was used to choose the optimal conformation. The dock results were ranked based on docking scores from high-low to identify the top-scoring compounds/ligands. The binding energy with more negative energy indicates a higher affinity of ligands bound to a receptor protein.

## 2.7 Molecular docking

Molecular docking studies were performed using the Autodock (<https://autodocksuite.scripps.edu/adt/>) for the top three compounds selected from virtual screening. The grid box was centered at X: 10.9010, Y: 1.4615, Z: 18.287, with dimensions (Å) of X: 60, Y: 60, Z: 60. Despite acknowledged limitations, such as the reliance on rigid protein structures and potential scoring function inaccuracies, docking remains a valuable tool for initial ligand screening. The results provide a rational basis for subsequent experimental work, aiding in the identification of potential drug candidates in the early stages of drug discovery (Sriramulu et al., 2021).

## 2.8 Molecular dynamic simulations

The structural and dynamic transitions at the atomistic level in the Mpro of COVID-19 upon binding of the top two molecules and two reference molecules were investigated using MD simulations. MD simulations were performed on GROMACS 2022.3 suite (<https://manual.gromacs.org/documentation/current/download.html>) (Abraham et al. 2015). On a LINUX based platform using CHARMM36 force field (Vanommeslaeghe et al., 2015). A Swiss-param server (<http://www.swissparam.ch/>) was used to generate the topology files of ligands (Zoete et al. 2011). A unit cell defined as a dodecahedron box was generated and solvated using the TIP3P water system. For the overall electrostatic neutrality of the system, 4 Na<sup>+</sup> was added. Then the electro neutral systems were energy minimized using the steepest descent algorithm for 250,000 iteration steps and cut-off up to 1000 kJ/mol to remove the bad contacts among the atoms. The energy-minimized systems were then subjected to two phases of equilibration for 250,000 steps. The first phase of equilibration (Temperature equilibration) was conducted under NVT ensemble for 500 ps to maintain the system temperature at 310 K using the V-rescale thermostat (Bussi et al., 2007) with a constant number of particles, volume, and temperature (NVT). Then second phase of equilibration (Pressure equilibration) was conducted under NPT ensemble for 500 ps to maintain a constant pressure of 1 bar for the system, using, Parinello-Rahman barostat with a constant number of particles, pressure, and temperature (NPT). For utilizing constraints of covalent bonds in the equilibration steps LINCS algorithm was used (Parrinello et al. 1981). To compute the long-range electrostatics forces using the Particle Mesh Ewald (PME) method with a Fourier grid spacing of 1.6 Å (Hess et al. 1997). After completion of the two equilibration phases, the systems were well-equilibrated and ready to run molecular dynamics (MD) for data collection thus a 200 ns MD simulation production run was carried out for each system on the NPT ensemble with step size 2 fs for each step. The coordinates were saved after every 10 ps during production run. Results were analyzed using the XMGRACE 2D plotting tool (Darden et al., 1993).

## 2.9 Binding free energy calculation

The molecular mechanics/Poisson-Boltzmann surface area (MM/PBSA) was used to compute residual binding energies in molecular interaction processes (Turner et al. 2005; Genheden et al., 2015; Sharma et al., 2020; Kumari et al., 2021; Singh et al., 2022a). The binding free energy ( $\Delta G_{\text{bind}}$ ) in a solvent medium was calculated as follows:

$$\Delta G_{\text{bind}} = G_{\text{complex}} - (G_{\text{protein}} + G_{\text{ligand}}) \quad (1)$$

In Equation (1),  $G_{\text{complex}}$  is the total free energy of the protein-ligand complex,  $G_{\text{protein}}$  and  $G_{\text{ligand}}$  are the total energies of protein and ligand, respectively. The binding free energies for each individual  $G_{\text{complex}}$ ,  $G_{\text{protein}}$  and  $G_{\text{ligand}}$  were calculated by:

$$G_p = \text{EMM} + G_{\text{solv}} \quad (2)$$

In Equation (2), p can be protein, ligand, or protein-ligand complex. EMM is the average molecular mechanics potential energy in vacuum and  $G_{\text{solv}}$  is the solvation free energy. The molecular mechanics potential energy was calculated in the vacuum as follows:

$$\text{EMM} = E_{\text{bonded}} + E_{\text{non-bonded}} \quad (\text{and } E_{\text{non-bonded}} = E_{\text{vdw}} + E_{\text{elec}}) \quad (3)$$

Here  $E_{\text{bonded}}$  is the total bonded interaction energy such as angle, bond, dihedral and improper interactions;  $E_{\text{non-bonded}}$  is the total non-bonded interaction energy that includes both van der Waals ( $E_{\text{vdw}}$ ) and electrostatic ( $E_{\text{elec}}$ ) interactions.  $E_{\text{bonded}}$  is taken as zero. The solvation free energy ( $G_{\text{solv}}$ ) is the sum of electrostatic solvation free energy ( $G_{\text{polar}}$ ) and nonpolar solvation free energy ( $G_{\text{non-polar}}$ ), which is computed using the Poisson-Boltzmann equation and the solvent-accessible surface area (SASA), respectively. The residual energy contribution was also calculated to understand the contribution of individual amino acids to the total binding energy.

### 3 Results and Discussion

The 3 chymotrypsin-like cysteine protease (Mpro) is the most desirable target for drug candidates against SARS-CoV-2 as it cleaves the C-terminal sequence of the polyprotein into functional proteins that play vital roles in viral replication, transcription and translation, leading to disruption of host cell metabolism. Hence, targeting Mpro can lead to developing protease inhibitors as effective therapeutic agents against SARS-CoV-2. It is a homodimeric protein consisting of three domains in each monomer; domain I (1–101), domain II (102–184), and domain III (201–304) (Fig. 1). The catalytic pocket consists of Gly143, His163, Asn142, Leu141, Phe140, Gly302, His172, Met165, Glu166, Pro168, Cys145, His164, Leu167, Pro168, Gln192, Asp187, Gln189, Phe185, Thr190, Ala191, His41, Met49 and Tyr54 amino acids (Singh et al., 2022b). In a study, Shitrit and co-workers discovered the conserved and essential amino acid interactions needed for developing potential inhibitors against Mpro target (Wang et al., 2020). These interactions included catalytic Cys145, conserved His163 and Glu166 residues hydrogen bond interactions with ligands/inhibitors. The reference drug used in the study was Baricitinib and Remdesivir as it was identified as an antiviral and anti-inflammatory drug against SARS-CoV-2 infection (Shitrit et al. 2020). Initially FDA approved Baricitinib along with Remdesivir for treatment of patient suffering from severe COVID 19, later it received FDA approval on July 28, 2021 for its single use and also recommended by the WHO (Kumari et al., 2022; Rubin et al., 2022). It suppresses the immersion of virus inside the host cell by interrupting the receptor-mediated endocytosis that leads to prevention of lungs from viral infections. Dual character (anti-viral-pathogen-centric drug and anti-inflammatory-host-centric) of Baricitinib attracted the attention of biologists towards its use against SARS-CoV-2 (Chera et al., 2022). Baricitinib is a medication that is primarily used to treat rheumatoid arthritis. However, during the COVID-19 pandemic, researchers explored its potential as an anti-inflammatory agent that could help mitigate the severe inflammatory response associated with severe cases of COVID-19. Baricitinib works by inhibiting certain enzymes involved in the inflammatory process, specifically Janus kinases (JAKs). The drug was used to reduce the excessive immune response seen in severe COVID-19 cases, potentially preventing further damage to the lungs and other organs. It was very useful in reducing the respiratory failure in COVID 19 patients, and does not show in major adverse effect except mild increase in liver enzyme. It also showed structural backbone similarity to most of the selected compounds. Baricitinib acts as Mpro inhibitor against the SARS-CoV-2 infection with IC<sub>50</sub> value of 25.31 μM (Anton et al. 2023). It also showed structural backbone similarity to most of the selected compounds. The cartoon structure of target protein, chemical structures of two references and top two shortlisted compounds are presented in Fig. 1. These two compounds (Norquinadoline A and Quinadoline B) also have common pyrimidine moiety like the two reference drugs, which is very important for the biological activity.

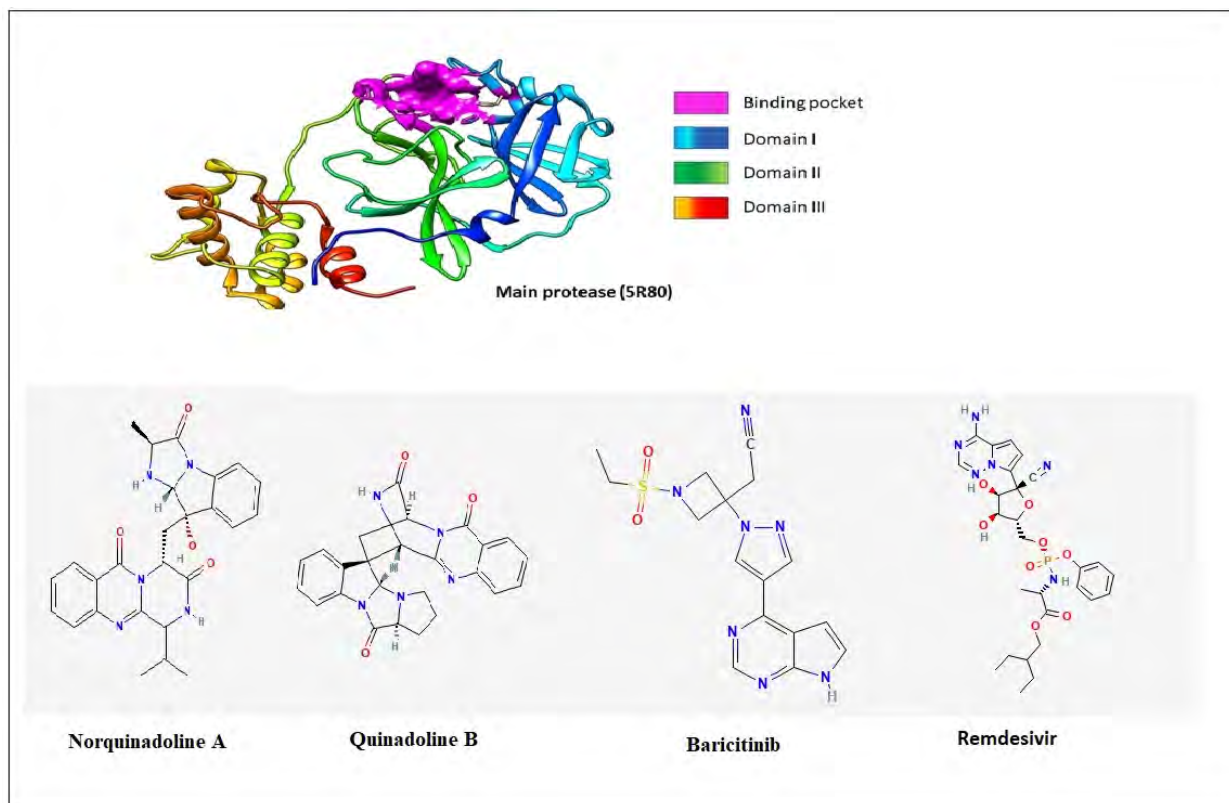


**Fig. 1** The 3-D cartoon view of SARS-CoV-2 main protease (Mpro) monomer showing different regions. The chemical structures of two references (Baricitinib and Remdesivir) and top two compounds (Norquinadoline A and Quinadoline B).

### 3.1 Analysis of physicochemical properties

The physicochemical properties of the top ten compounds followed Lipinski's rule of five presented in Table 1. The top ten compounds showed the hydrogen bond acceptor and hydrogen bond donor were found to be in acceptable range, log P value (lipophilicity) was less than 5, and total polar surface area (TPSA) was less than 140. Lower values of lipophilicity referred to good internalization of all compounds through cell membrane and lower value of TPSA referred to easy incorporation of compounds in human cells like the reference drug. The compounds showing more than one violation of Lipinski's rule were removed from further studies because of difficulty in solubility and bioavailability.

**Table 1** Physicochemical properties of the top ten compounds and two reference compounds.

Compounds	MW <500	H-D ≤5	H-A ≤10	Rotatable bonds ≤10	Log P ≤5	TPSA ≤140	SAS ≤10	Log S ≤5	Log Kp <-5	ROF ≤1
Norquinadoline A	471.5	3	6	2	1.97	116.56	4.92	-4.00	-8.01	0
Scedapin A	472.5	2	7	0	2.06	113.77	5.50	-3.84	-8.35	0
Protopine	353.4	0	6	0	2.75	57.24	3.48	-4.13	-6.47	0
Withaferin A	470.6	2	6	3	3.83	96.36	6.83	-4.97	-6.45	0
Cottoquinazoline B	429.43	2	6	0	2.12	107.77	4.72	-3.21	-8.54	0
Silybin	482.4	5	10	4	1.47	155.15	4.92	-4.14	-7.89	0
Quinadoline B	439.5	1	5	0	1.36	87.54	5.31	-3.09	-7.82	0

Tingenone	420.6	1	3	0	4.03	54.37	5.94	-5.40	-5.34	0
Licoleafol	372.4	5	7	4	2.64	127.45	3.82	-3.91	-6.65	0
10-methoxycamptotheci n	378.4	1	6	2	2.06	90.66	3.94	-3.55	-7.39	0
Reference compound 1 (Baricitinib)	371.0	1	7	5	-0.24	120.57	3.07	-1.92	-8.89	0
Reference compound 2 (Remdesivir)	602.58	4	12	14	3.46	213.36	6.43	-4.12	-8.62	0

MW: Molecular weight; H-A: number of H bond acceptors; H-D: number of H bond donors; Log P: predicted octanol-water partition coefficient; TPSA: total polar surface area; ROF: Rule of five, Log S predicted aqueous solubility, Log Kp predicted skin permeability, SAS (Synthetic accessibility score) from 1 (very easy) to 10 (very difficult).

### 3.2 Analysis of drug-likeness properties

The bioactivity scores, namely G-protein coupled receptor (GPCR) ligand, ion channel modulator, kinase inhibitor, nuclear receptor ligand, protease inhibitor, and enzyme inhibitor were calculated to evaluate drug-like properties of top ten compounds (Table 2). The compounds showing bioactivity score more than zero to be considered as pharmaceutically active compounds, whereas the compounds show bioactivity score between 0.00 and -0.50 supposed to best moderate activity and then bioactivity score <-0.50 means no bioactivity. On the analysis of results, it was found that the top-ten compounds exhibit good to moderate bioactivity scores and therefore showed good to moderate drug-like properties. Results are summarized in Table 2.

Brain access and gastrointestinal absorption are important drug-like properties, which is very crucial for the drug development process (Singh et al. 2022b). The prediction of these two properties presented through the BOILED-Egg model in Fig. 2 (Singh et al., 2024). Except compounds **3** and compound **6**, all compounds that were present in white zone, can be easily absorbed by the gastrointestinal tract like the reference compound **1**. Compound **3** was present in the yellow zone and can easily pass through the blood brain barrier. Reference compound **2** is out of range in the BOILED-Egg model.

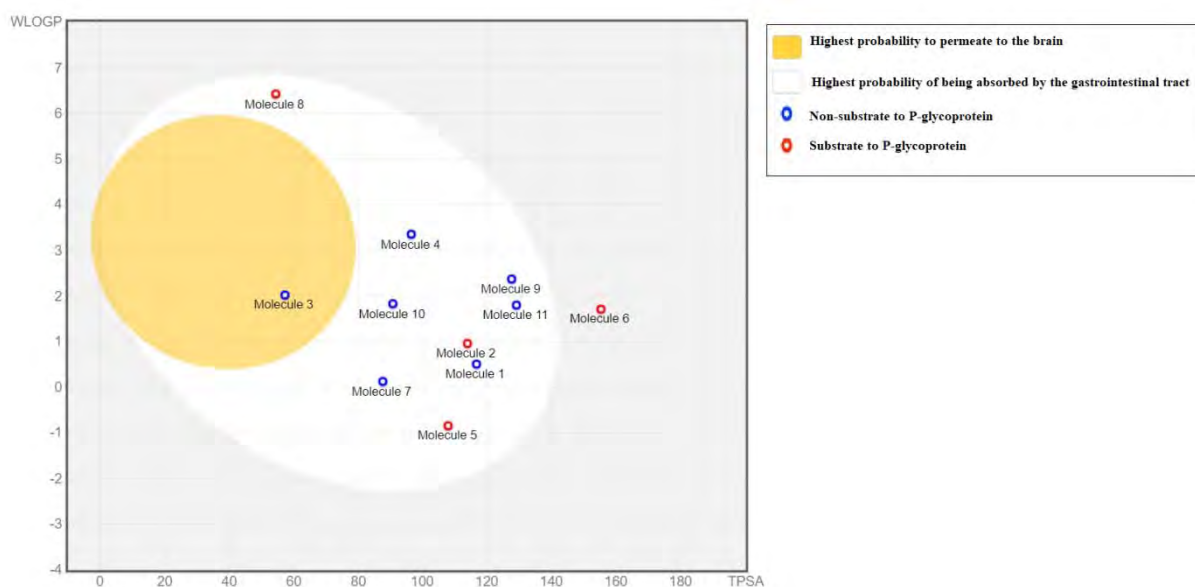


**Fig. 2** BOILED-Egg presentation of the top ten compounds (**1-10**) and the reference compound **1** (**11**).

**Table 2** Drug-likeness properties of the top ten compounds and two reference compounds.

Compound	GPCR ligand	Ion channel modulator	Kinase inhibitor	Nuclear receptor ligand	Protease inhibitor	Enzyme inhibitor
Norquinadoline A	0.09	-0.41	-0.50	-0.48	-0.30	-0.23
Scedapin A	0.14	-0.25	-0.33	-0.28	-0.25	-0.11
Protopine	0.18	-0.04	-0.26	-0.23	-0.03	0.04
Withaferin A	0.07	0.14	-0.49	0.76	0.15	0.94
Cottoquinazoline B	0.10	-0.48	-0.52	-0.55	-0.21	-0.19
Silybin	0.07	-0.05	0.01	0.16	0.02	0.23
Quinadoline B	0.14	-0.29	-0.36	-0.43	-0.09	-0.14
Tingenone	-0.20	-0.26	-0.40	0.48	-0.17	0.53
Licoleafol	0.25	-0.10	-0.06	0.71	0.11	0.52
10-methoxycamptothecin	0.39	-0.20	0.24	0.07	-0.16	1.00
Reference compound 1 ( <b>Baricitinib</b> )	0.27	-0.12	0.62	-0.76	-0.03	0.11
Reference compound 2 ( <b>Remdesivir</b> )	0.27	-0.35	0.20	-0.48	0.49	0.38

GPCR (G-protein coupled receptor-ligand): (-0.62 to -0.39, moderate activity), Ion channel modulator: (0.27 to 0.05, significant activity), Protein kinase inhibitors: (0.40 to 0.18, significant activity), Nuclear receptor: (-0.63 to -0.31, moderately active), Protease activated receptors: (-0.15 to 0.00, moderate activity) and Enzyme inhibitor: (0.61 to -0.48, significant activity).

### 3.3 *In silico* ADMET prediction

ADMET properties, such Absorption (viz., water solubility, intestinal absorption (%) and skin permeability (log Kp)), Distribution (log BB), Metabolism, Excretion (viz., total clearance and renal OCT2 substrate), and Toxicity (viz., oral rat acute toxicity LD<sub>50</sub>, maximum tolerated dose in human, and synthetic accessibility) parameters of the top ten compounds and two reference compounds were computed and presented in Table 3. Nine natural compounds qualified the drug-like criteria of  $\geq 70\%$  absorption. Water solubility results indicated the good drug bioavailability as the compounds showed water solubility value  $\leq -5$  (Daina et al. 2016). Skin permeability (log Kp) plays a significant role in transdermal delivery of drugs and the compounds showing higher negative value of log Kp have lower skin permeability. All the compounds showed good permeability as value ranged between -2.73 to -3.20. All compounds were expected to cross the blood brain barrier easily as their log BB values were  $< -0.1$  (Chen et al., 2018; Vilar et al., 2010). Bioavailability of drugs is also influenced by metabolism of the drug molecules and this can be evaluated by using cytochrome CYP450 enzymes. On analysis, all the top ten compounds and two reference drugs Baricitinib and Remdesivir were found to be inhibitors of one of the cytochrome variants. All ADMET properties were found to be favorable for all the top ten compounds. Blood brain barrier access and intestinal absorption are two major drug-like behaviors critical to estimate at various stages of drug discovery processes. The results of drug-likeness and ADMET properties are summarized in Tables 3 and 4.



**Table 4** Toxicity prediction of the top ten compounds and two reference compounds.

Compound	AMES Toxicity Categorial (Yes/No)	Max. tolerated dose(human) Numeric (log mg/kg/day)	hERG Inhibitor Categorial (Yes/No)	Oral Rat Toxicity Numeric mg/kg/day)	Chronic (LOAEL) (log	Hepatotoxic ity Categorial (Yes/No)	Skin Sensation Categorial (Yes/No)	T. Pyriformis toxicity Numeric (log mM)	Minnow Numeric (log mM)
Norquinadoline A	N	-0.12	N	2.689		Y	N	0.285	1.697
Scedapin A	N	0.161	N	1.842		Y	N	0.285	0.335
Protopine	Y	-0.446	N	1.93		N	N	0.64	1.237
Withaferin A	N	-0.695	N	0.918		N	N	0.299	0.738
Cottoquinazoline B	N	-0.233	N	1.832		Y	N	0.285	1.399
Silybin	N	0.65	N	3.494		N	N	0.285	2.543
Quinadoline B	N	0.163	N	1.162		Y	N	0.285	1.364
Tingenone	N	-0.84	N	1.85		N	N	0.497	-0.245
Licoleafol	N	0.284	N	2.517		N	N	0.369	3.528
10-methoxycamptothecin	N	-0.074	N	1.456		Y	N	0.295	-0.477
Reference compound 1 ( <b>Baricitinib</b> )	N	-0.111	N	1.539		Y	N	0.296	1.769
Reference compound 2 ( <b>Remdesivir</b> )	N	0.15	N	1.639		Y	N	0.285	0.291

LD50 (Lethal Dose) = Lower value predicts minimum toxicity; Maximum tolerated dose =  $\leq 0.47$  predicts lower toxicity; AMES = Mutagenic or carcinogenic toxicity; LOAEL (Lowest adverse effect level test =  $LOAEL \leq 10$  mg per kg per day were labeled as strong chronic toxicity, chemicals with  $LOAEL > 50$  mg per kg per day were labeled as weak chronic toxicity and chemicals with LOAEL ranged from 10 to 50 mg per kg per day were labeled as medium chronic toxicity; T. Pyriformis toxicity = Tetrahymena Pyriformis toxicity; Minnow toxicity = Acute fathead minnow toxicity is the basis of hazard and risk assessment for compounds in the aquatic environment. Structure–minnow toxicity relationship as follows:  $\log LC50 = -0.94 \log p + 0.94 \log (0.000068 p + 1) - 1.25$  where p is the n-octanol/ water partition coefficient.

### 3.4 Virtual screening analysis

Virtual screening, a widely utilized computational tool, plays a crucial role in predicting binding energy across diverse complexes such as protein-ligand, protein-protein, and RNA-ligand interactions. Through virtual screening 57 compounds were docked with Mpro protein and top ten compounds were selected on the basis of high negative binding energy compared to reference. Out of the top 10 potential SARS-CoV-2 inhibitors the four are mycochemicals and six are phytochemicals (Table 5). All the top ten compounds showed better binding affinity to Mpro than reference indicating their probable potency as Mpro inhibitor. The binding energy of two reference compound Baricitinib and Remdesivir is -7.5 kcal/mol and -8.1 kcal/mol respectively, which is lower than the binding energies of the top two compounds; compound **1** (Norquinadoline A) and compound **2** (Quinadoline B) with highest binding energy -10.0 kcal/mol, -10.2 kcal/mol, respectively (Table 5). The strong binding energy reflects strong interaction between the ligand/compounds and Mpro binding pocket residues. These interactions include both hydrogen bonds interactions and non-bonded interactions. The compound's interactions with SARS-CoV-2 Mpro residues are shown in (Table 5). Compound **1** formed one conventional hydrogen bonds at Asn142(A) and non-bonded interactions at Met 49(A), Met 165(A), Met 49(A), Pro 168(A), Glu 166(A), whereas compound **2** formed three conventional hydrogen bonds at Asn 142(A), Glu 166(A), His 41(A) and non-bonded interactions at Met 49(A), Cys 145(A), Met 49(A), Glu 166(A), His 41(A). These interactions were comparable to the reference compound **1** that formed five hydrogen bonds at Phe 140(A), Glu 166(A), Pro 168(A), Glu 166(A), Gln 189(A), and non-bonded interactions at Glu 166(A) and reference compound **2** that formed four hydrogen bonds Cys 145(A), His 41(A), Cys 145(A), Glu 166(A), and non-bonded interactions at His 41(A), Met 49(A), His 41(A), Met 165(A), Thr 25(A), Leu 141(A), Gly 143(A), Thr 25(A), Thr 24(A) though the interacting binding pocket residues are different in all three complexes (Fig. 3 and Fig. 4). The observed hydrogen bond interactions in the binding pocket are biologically relevant due to their crucial role in stabilizing the protein-ligand complex. Hydrogen bonds play a key role in molecular recognition and binding specificity, contributing to the overall binding affinity. The specificity and strength of hydrogen bonding interactions can influence the ligand's ability to form a stable complex with the protein, impacting its biological activity and therapeutic potential.

**Table 5** Virtual screening result of the top ten compounds and two reference compound complexes.

Compound	Binding energy (kcal/mol)	No. of H-bonds	H-bond interaction	Non-bonded interaction	No. of interacting amino acids
Quinadoline B	-10.2	3	Asn 142(A)	Met 49(A)	7
			Glu 166(A)	Cys 145(A)	
			His 41(A)	Met 49(A)	
				Glu 166(A)	
				His 41(A)	
Norquinadoline A	-10.0	1	Asn 142(A)	Met 49(A)	6
				Met 165(A)	
				Met 49(A)	
				Pro 168(A)	
				Glu 166(A)	
Scedapin A	-9.2	3	Gln 110(A)	Val 104(A)	6
			Ser 158(A)	Arg 298(A)	
			Arg 298(A)	Asp 153(A)	

Protopine	-8.8	6	Asn 142(A) Glu 166(A) Asn 142(A) His 41(A) Asp 187(A) Gln 189(A)	Met 49(A) His 41(A) Met 49(A) Glu 166(A) Met 49(A) Cys 145(A)	12
Withaferin A	-8.8	3	Asn 142(A) Leu 287(A) Leu 271(A)	Leu 286(A) Tyr 239(A) Leu 286(A) Leu 272(A) Leu 286(A) Tyr 237(A)	9
Cottoquinazoline B	-8.8	1	Glu 166 $\bar{A}$	Met 49(A) Met 165(A) Met 49(A)	4
Silybin	-8.6	6	Thr 24(A) Thr 26(A) Glu 166(A) Met 165(A) Asp 187(A) Thr 24(A)	Met 49(A) His 41(A) Cys 145(A) Thr 24(A) His 41(A)	11
Tingenone	-8.3	3	Gly 275(A) Lys 137(A) Gly 275(A)	Leu 286(A) Leu 287(A) Leu 272(A) Tyr 239(A)	7
Licoleafol	-8.2	6	Cys 143(A) Glu 166(A) His 164(A) His 41(A) Thr 25(A) His 41(A)	Met 49(A) His 41(A) Cys 145(A) Met 49(A)	10
10-methoxycamptothecin	-8.1	7	Thr 26(A) Gly 143(A) Leu 141(A) His 163(A) Glu 166(A) Met 165(A) Cys 145(A)	His 41(A)	8
Reference compound (Baricitinib)	-7.5	5	Phe 140(A) Glu 166(A) Pro 168(A) Glu 166(A) Gln 189(A)	Glu 166(A)	6

Reference compound 2 (Remdesivir)	-8.1	4	Cys 145(A) His 41(A) Cys 145(A) Glu 166(A)	His 41(A) Met 165(A) His 41(A) Met 165(A) Thr 25(A) Leu 141(A) Gly 143(A) Thr 25(A) Thr 24(A)	13
--------------------------------------	------	---	---	---	----

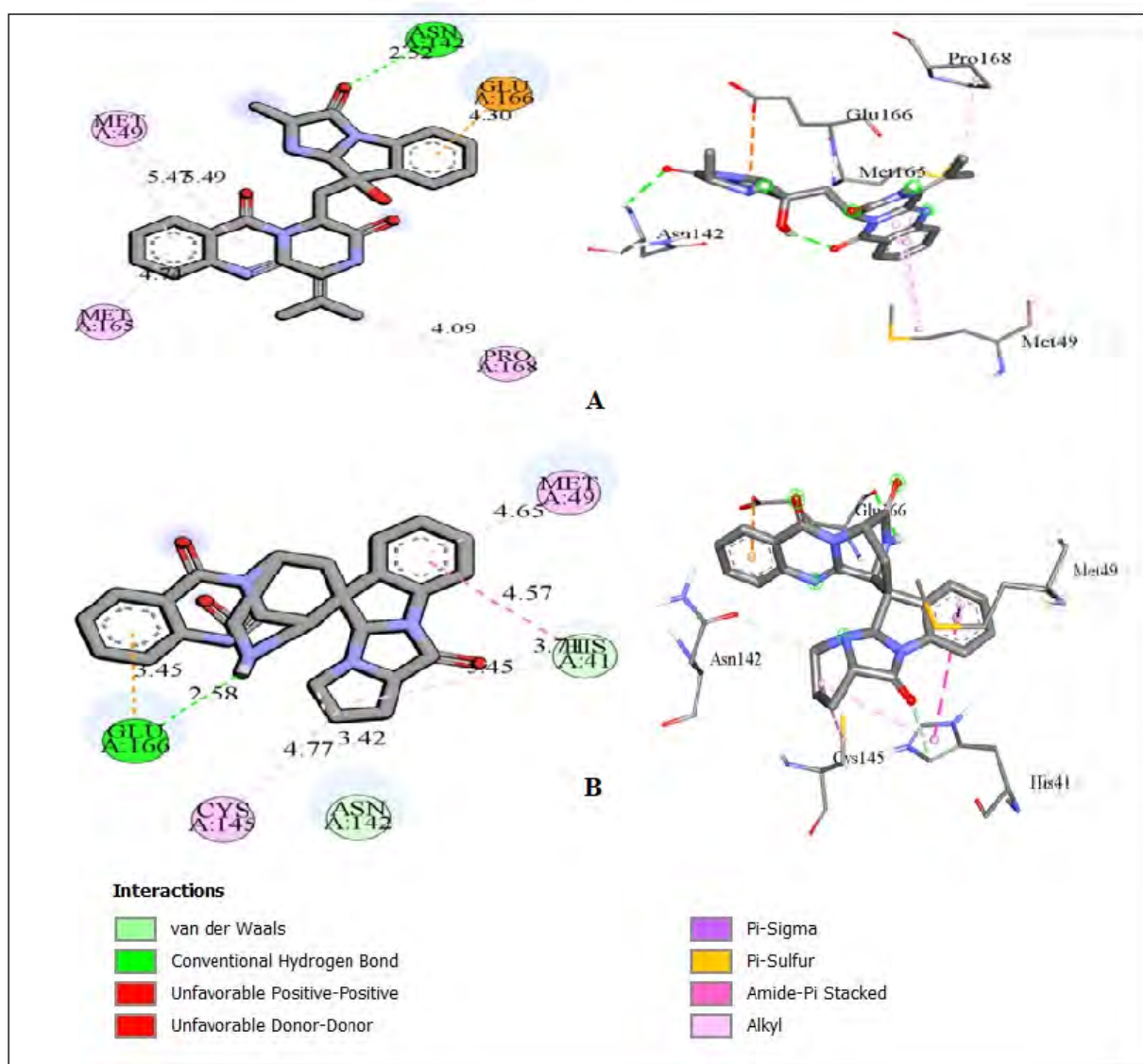


**Fig. 3** Protein-ligand interactions (2D view and 3D view) of the top two complexes; (A): Compound 1 complex (B): Compound 2 complex.

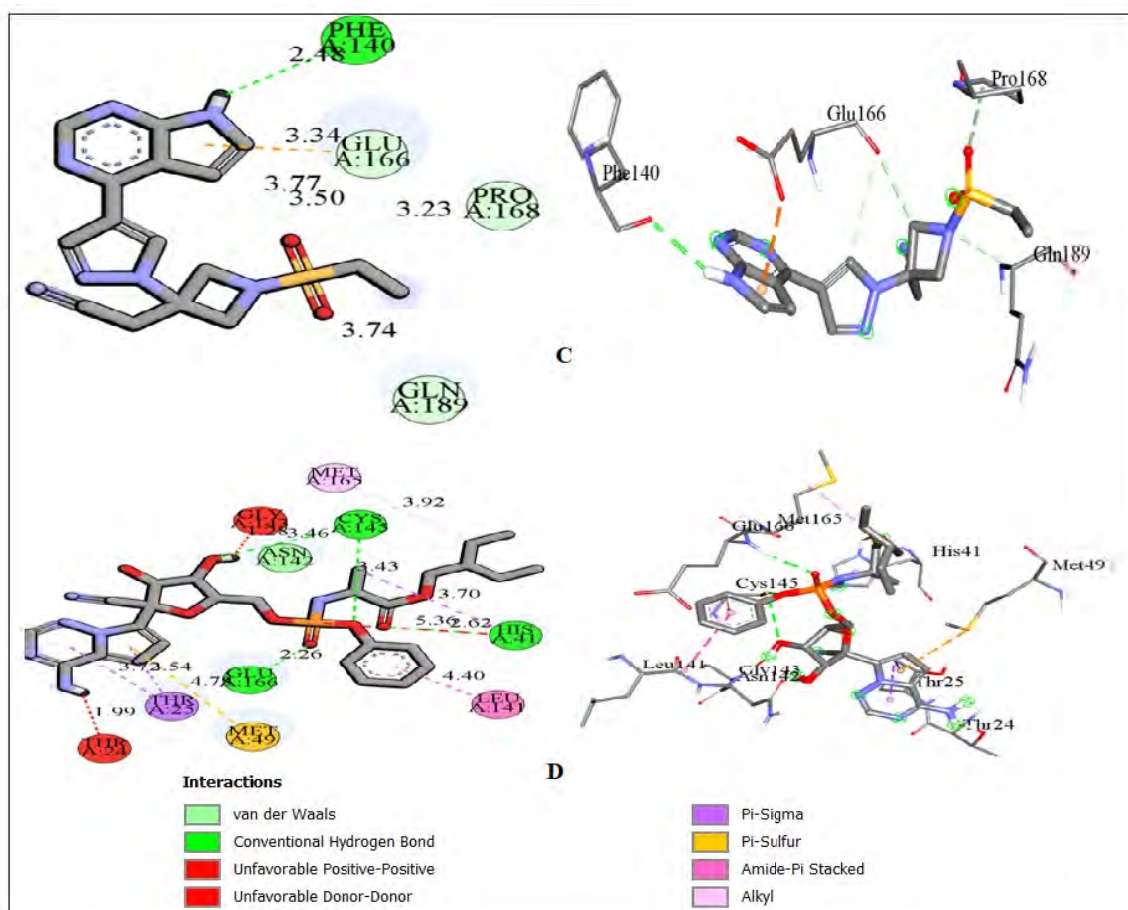


**Fig. 4** Protein-ligand interactions (2D and 3D view) of the two References; (C): Reference Complex 1 and (D): Reference complex 2.

### 3.5 Molecular docking analysis

After the analysis of virtual screening results, the top two compounds were subjected to molecular docking analysis on the basis of their binding affinity. Here compound **1** (Norquinadoline A) and compound **2** (Quinadoline B) were used as ligands and their versatile binding poses with SARS-COV 2 Mpro were explored which revealed compound **1** (Norquinadoline A) exhibited phenomenal binding with binding energy of **-10.65**, while compound **2** (Quinadoline B) also manifested a binding energy of **-10.24** (Table 6).

**Table 6** Binding energy of the putative drug candidates after molecular docking

Compound	Binding Energy (kcal/mol)	Reference RMSD
Norquinadoline A	-10.65	18.41
Quinadoline B	-10.24	10.38

The molecular docking analysis showed that compounds **1** and compound **2** were extensively involved in binding with target protein Mpro, and their complexes with Mpro were more stable as compared to the complex

formed between the reference drug Baricitinib and Mpro. Since the molecular docking studies were used to determine the stability of the complex formed between the compounds and target protein in a fixed pose, but its stability was affected by the physiological conditions and time. Therefore, for further validation of stability of the complexes, MD studies were performed on the selected complexes.

### 3.6 Molecular dynamics studies

We combined molecular dynamics simulations and energy analysis to elucidate the stability of the docked complexes and mechanism underlying the binding of compound **1**, compound **2** and two reference compounds to Mpro target. MD simulations were performed for 200 ns and then trajectories were further analysed.

#### 3.6.1 Structural stability and flexibility analysis

The Root Mean Square Deviation (RMSD) graph illustrates initial fluctuations, stabilizing after 50 ns and maintaining stability till 200 ns, followed by subsequent fluctuations for compound **1** and compound **2** complexes (Fig. 5A). The average RMSD values for all complexes, namely compound **1**, compound **2**, Reference compound **1**, and Reference compound **2** are 0.20 nm, 0.15 nm, 0.22 nm, and 0.23 nm respectively. These findings suggest that all complexes maintain stable structures with minimal conformational changes resulting from the binding of different compounds. Notably, the RMSD trajectory after 150 ns for compound **2** and Reference compound **2** exhibits similar fluctuations, attributed to their close structural resemblance (Fig. 5). The Root Mean Square Fluctuation (RMSF) graph captures the flexibility of residues during the simulation (Fig. 5B). All complexes exhibit a similar fluctuation profile, indicating uniform flexibility of alpha carbon atoms in the residues. Compound **1** demonstrates lower fluctuations compared to compound **2** and the reference, signifying greater stability. The residues within the binding pocket remain stable with minimal fluctuations, while higher fluctuations are observed for compound **2** and Reference compound **2**, particularly at the terminals of all complexes. Overall, these observations suggest the formation of stable and flexible complexes. Furthermore, the RMSD analysis of the protein backbone during the MD simulation reveals notable fluctuations, particularly between 150 to 180 ns (Fig. 5A). The RMSF analysis of the alpha carbon backbone atoms also exhibits fluctuations, with peaks reaching 2 nm (Fig. 5B). These fluctuations indicate dynamic structural changes during specific time intervals, contributing to the overall understanding of the protein's behavior and flexibility throughout the MD simulation.

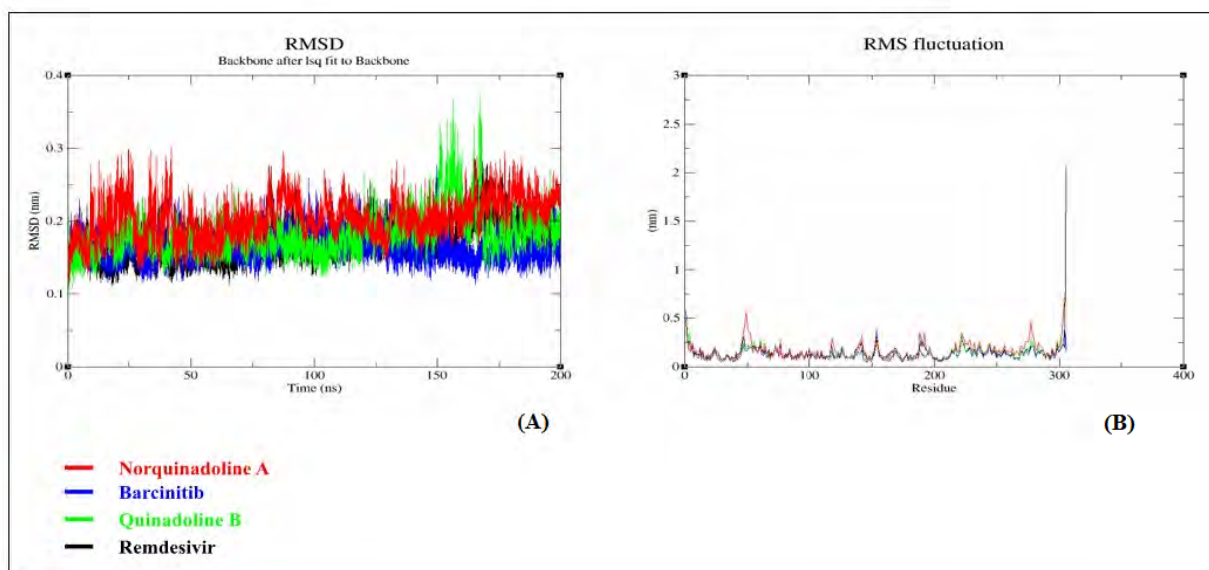


**Fig. 5** (A) RMSD analysis of the protein backbone during MD simulation. (B) RMSF analysis of the alpha carbon backbone atoms of the four complexes.

### 3.6.2 Ligand dynamics

We investigated the conformational dynamics of each ligand in the three complexes by calculating the corresponding RMSD of heavy atoms, as shown in Fig. 6. The movement of ligand in the binding pocket along the entire simulation indicates that the compound1 and 2 both showed a pose change after 50 ns and then remained stable in the binding pocket while the reference compound 1 exhibited almost no conformational changes throughout the simulation while reference compound 2 exhibited stable changes in conformation for the major part of the simulation but some instability was observed between 150 to 180 ns. This is possible as the reference compound is smaller in chemical structure compared to bulky compound 1 and compound 2, so the reference compound exhibits different poses.

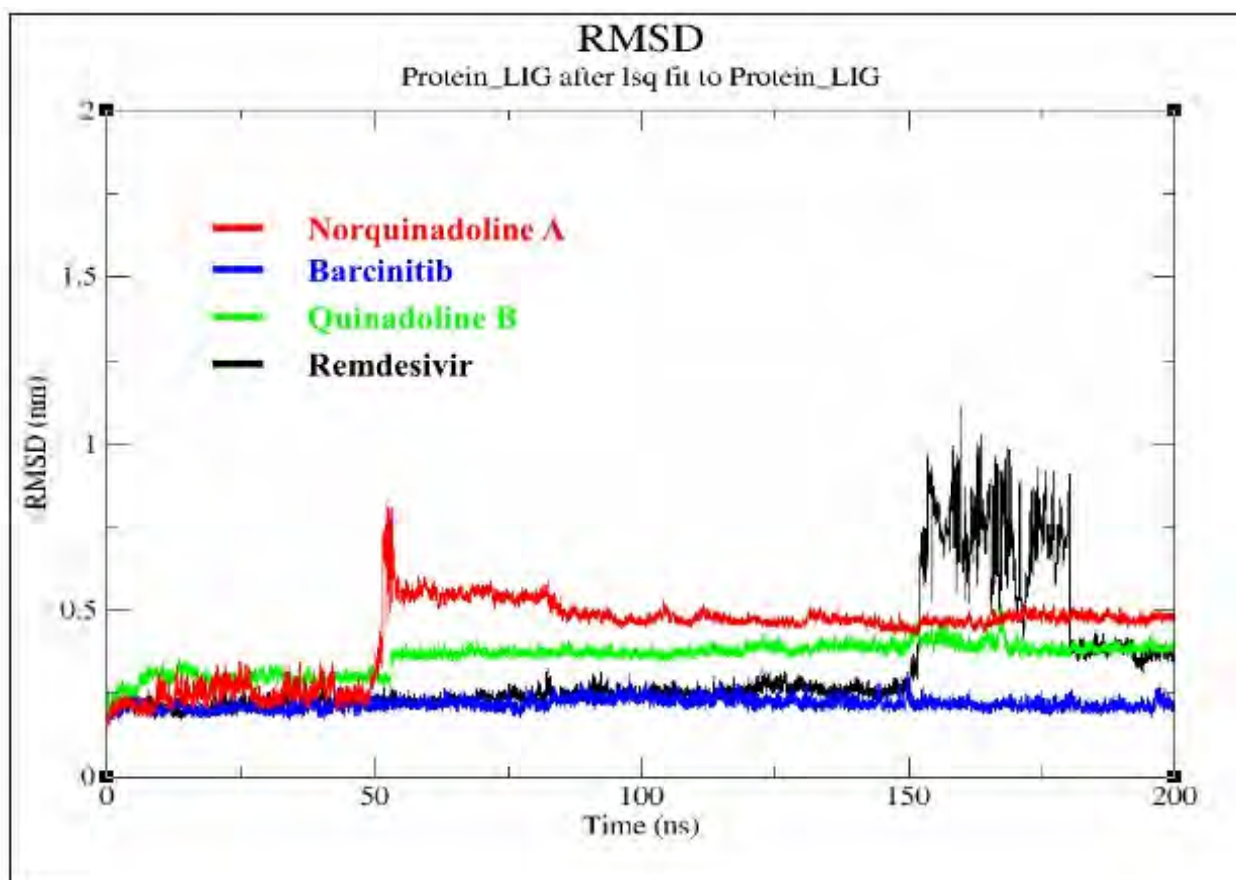


**Fig. 6** RMSD analysis of all the four compounds in the binding over the entire MD simulation.

### 3.6.3 Hydrogen bond analysis

The hydrogen bond analysis of the three complexes revealed distinct temporal profiles. Reference and compound **1** displayed higher hydrogen bond counts, whereas compound **2** exhibited a decrease in hydrogen bonds over time (Fig. 7). Notably, the hydrogen bonds in the reference complexes were less stable, indicating varying ligand poses near the binding pocket and supporting observations in ligand dynamics. In contrast, both compound **1** and compound **2** exhibited stable hydrogen bond profiles, suggesting a consistent and enduring interaction. The volatile hydrogen bond profile in the reference compounds aligns with diverse ligand poses, emphasizing the dynamic nature of ligand binding in the vicinity of the binding pocket. Overall, our findings highlight that the complex involving compound **1** demonstrated a stable and higher number of hydrogen bonds throughout the simulation, indicative of a robust and inhibitory binding interaction.

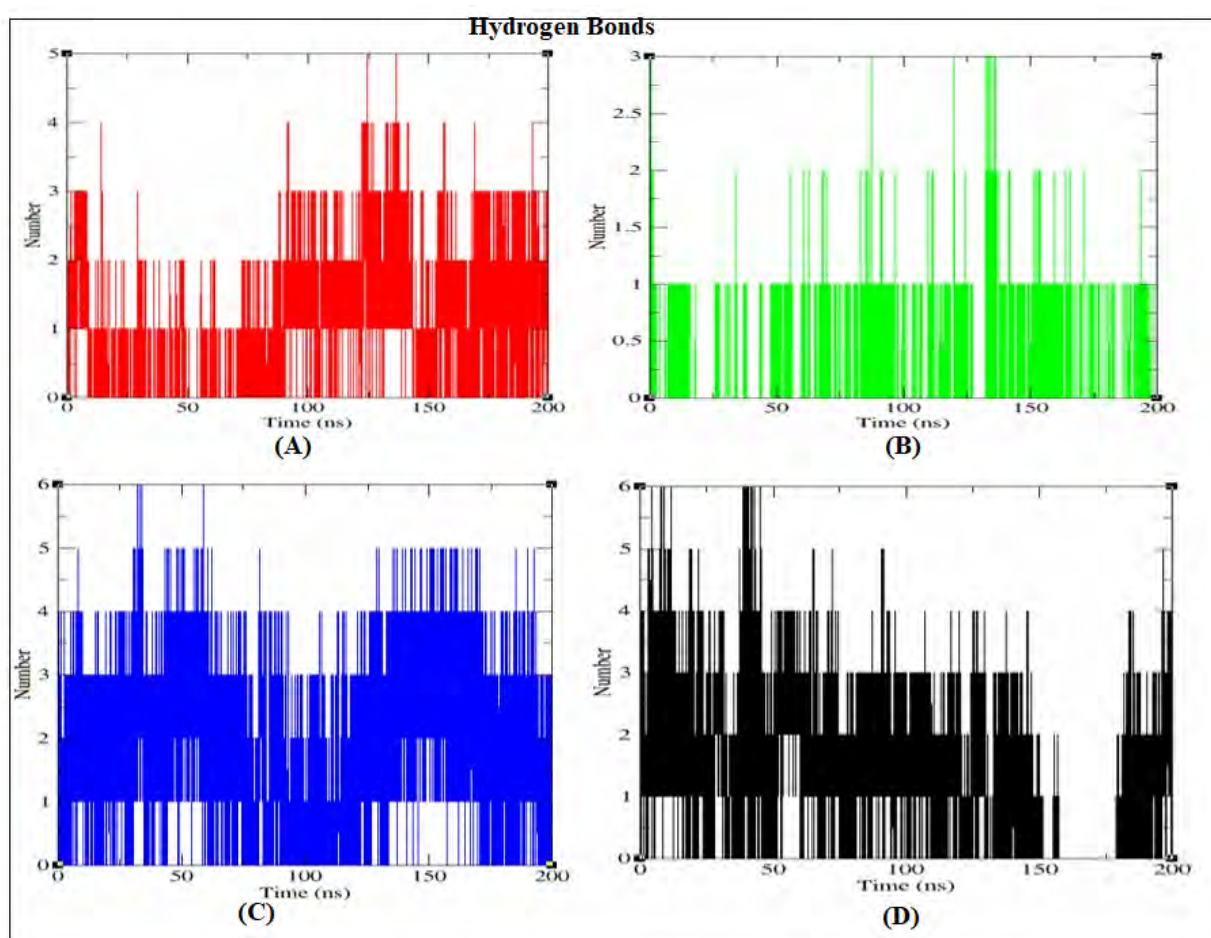


**Fig. 7** Hydrogen bond profiles over simulation times for all four complexes: (A) Compound **1**, (B) Compound **2**, (C) Reference compound **1**, and (D) Reference compound **2**.

### 3.6.4 Compactness and solvated surface analysis

The system's compactness over the simulation time was assessed through the Radius of Gyration ( $R_g$ ). A higher  $R_g$  value implies reduced compactness (more unfolded) and increased conformational entropy, while a lower  $R_g$  value signifies excellent compactness and structural stability (more folded). In our analysis, compound **1** and compound **2** and reference complexes exhibited comparable compactness, with Compound **1** displaying increased compactness in the last 50 ns, indicating a conformational change (Fig. 8). The Solvent

Accessible Surface Area (SASA) graph supported the observed compactness, as an increase in compactness corresponded to a reduction in surface residues exposed to water. Both the Rg and SASA results collectively indicated that the binding of these two compounds (compound **1** and reference compound **1**) did not induce significant structural changes.

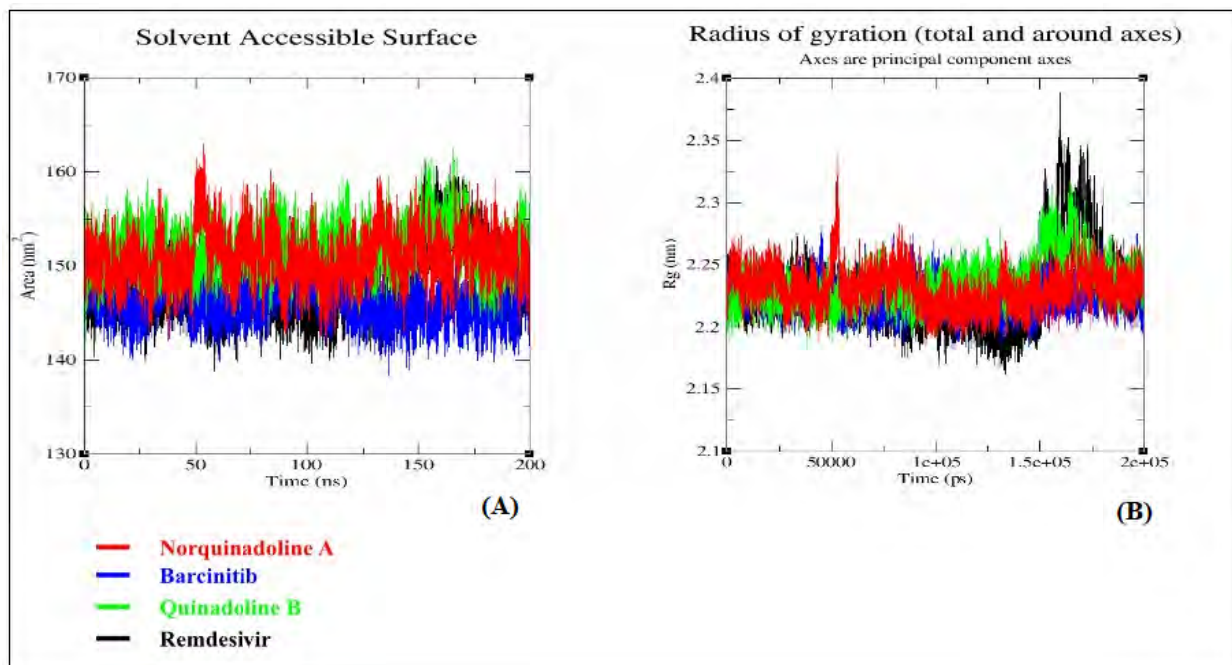


**Fig. 8** (A) SASA and (B) Radius of gyration profile of all four complexes.

### 3.6.5 Free energy landscape (FEL)

The Free Energy Landscape (FEL) serves as a crucial tool for elucidating energy barriers within conformational basins, offering insights into the structure-function relationships of proteins. It is commonly employed to analyze the lower energy minima conformations of proteins during molecular interactions, particularly in the context of different inhibitor bindings. In this study, we utilized the FEL graph to comprehend the conformational dynamics of Mpro following various inhibitor bindings. The FEL graph was constructed using the first two principal components (PC1, PC2) as collective variables, as depicted in Fig. 9 A–D. Principal Component Analysis (PCA) was employed to generate the principal modes that contribute to the functional dynamics of complexes across all systems. MD trajectories were utilized in PCA, with a focus on the Ca atom, providing a comprehensive understanding of the conformational changes induced by inhibitor bindings in Mpro.

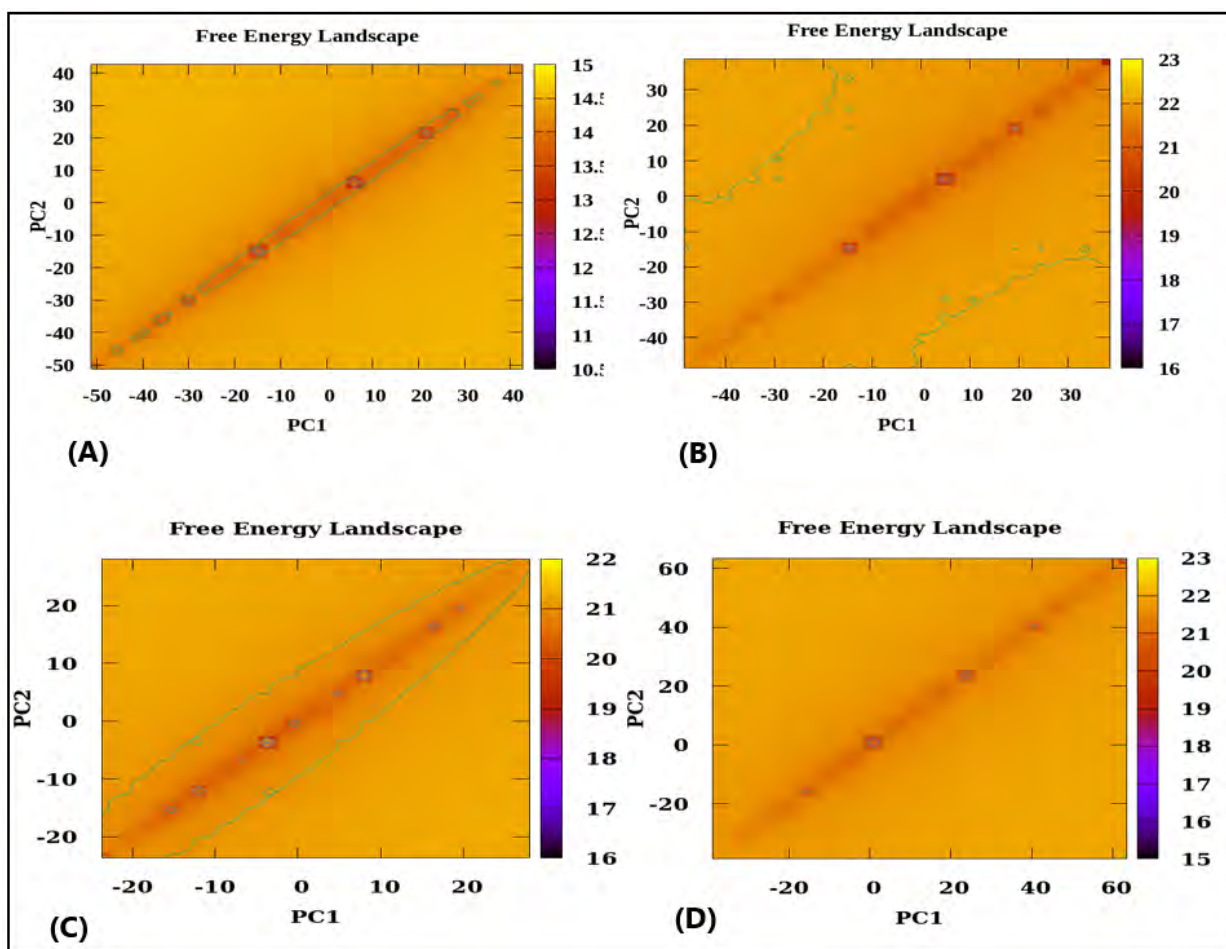


**Fig. 9** (A) Free energy landscape of all four complexes (Compound 1 (A), Compound 2 (B), and Reference compound 1 (C) and Reference compound 2 (D)).

### 3.6.6 Energetics of inhibitor binding to Mpro

MM/PBSA approach was routinely used to calculate binding free energy from MD trajectory. The binding free energy of both complexes was calculated using the *gmx\_mmpbsa* method from 600 snapshots extracted at equal intervals of 50-200 ns of stable MD trajectories. The contributions of different interactions to the binding free energy have been summarized in Table 7. Compound 1 and compound 2 showed high total binding free energy compared to reference compound 1 while reference compound 2 showed the highest total binding free energy due to its high molecular weight, not following Lipinski's rule of five. This indicates that compound 1, compound 2, and reference compounds binds strongly to Mpro. Decomposition into separate energy terms showed that the polar solvation energy decreases the binding strength of inhibitors to the protease significantly, and thereby reduces the total binding energy in both compound 1 and compound 2 and reference complexes due to the positive energy contributions (Table 7). Among the various interactions, van der Waal molecular mechanics energy, electrostatic molecular mechanics energy, Polar and Non-polar contribution to the solvation-free energy, total gas phase molecular mechanics energy, total solvation energy, and total binding free energy showed the most favorable contributions towards the negative binding free energy. The energy per residue was also generated to detect the key residues responsible for binding interaction with compound 1, compound 2, and the reference drug (Fig. 10-11). Compound 1

(Norquinadoline A) emerges as a potential lead compound due to its notably high total binding free energy (-20.19 kcal/mol) and low interaction entropy (2.77 kcal/mol), suggesting strong binding affinity and a degree of binding flexibility, respectively, towards the target Mpro.

**Table 7** Interaction energies of the two top compound complexes and reference complexes (kcal/mol).

Energy (kcal/mol)	Component	Compound1 (Norquinadoline A)	Compound 2 (Quinadoline B)	Reference (Baricitinib)	Reference 1	Reference 2 (Remdesivir)
$\Delta$ VDDWAALS		-31.05	-23.93	-34.06		-61.59
$\Delta$ EEL		-15.70	-10.26	-13.93		-24.81
$\Delta$ EGB		26.61	21.94	37.79		51.71
$\Delta$ ESURF		-3.82	-2.91	-4.42		-7.67
$\Delta$ GGAS		-46.75	-34.19	-47.99		-86.40
$\Delta$ GSOLV		23.79	19.03	33.38		44.04
$\Delta$ TOTAL		-22.96	-15.16	-14.62		-42.36
$\Delta$ G		-20.19 +/- 2.87	-7.41 +/- 4.27	-13.13 +/- 2.18		-37.46 +/- 4.30
-T $\Delta$ S		2.77	7.75	1.49		4.90

$\Delta$ VDDWAALS: van der Waals molecular mechanics energy,  $\Delta$ EEL: Electrostatic molecular mechanics energy,  $\Delta$ EPB: Polar contribution to the solvation energy,  $\Delta$ ESURF: Non-polar contribution to the solvation free energy,  $\Delta$ GGAS: Total gas phase molecular mechanics energy,  $\Delta$ GSOLV: Total solvation energy,  $\Delta$ TOTAL: total binding free energy,  $\Delta$ G: Binding free energy. -T $\Delta$ S: Interaction Entropy.

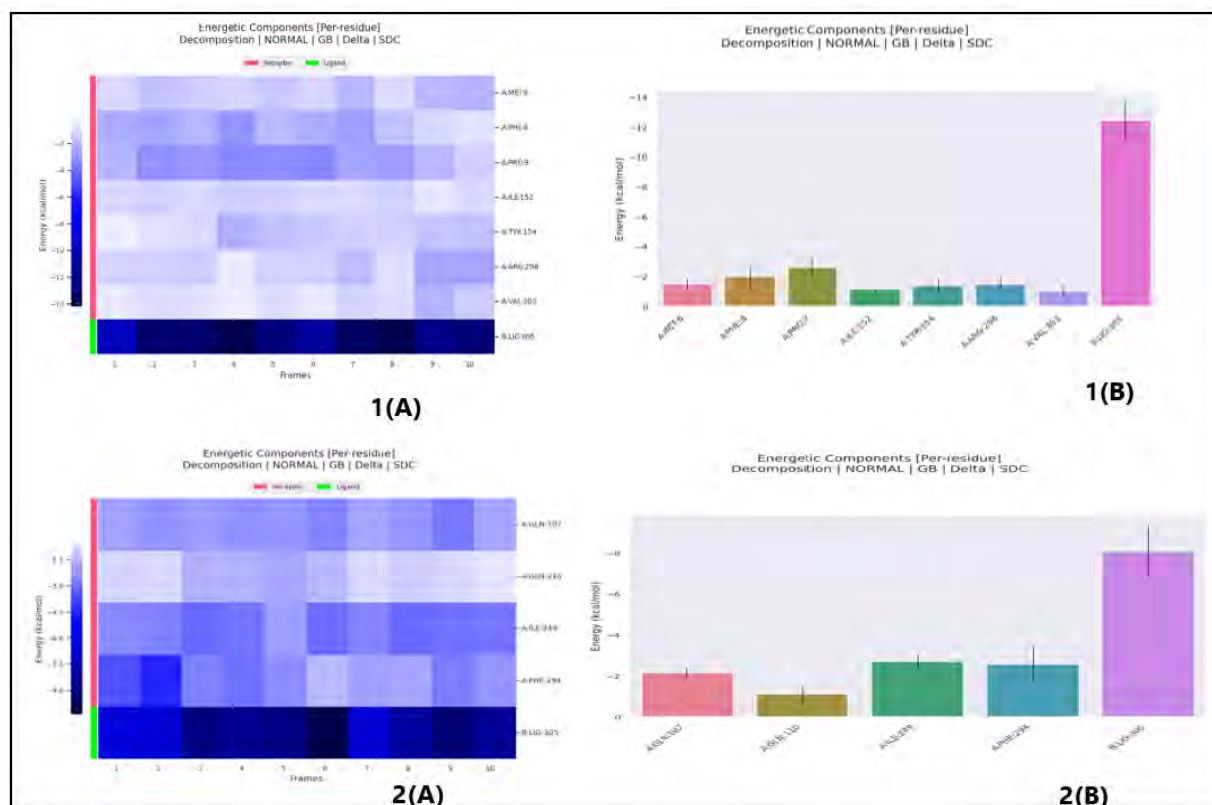


**Fig. 10** (A) Per-residues decomposition result of all two complexes (Compound 1 (A-B), Compound 2 (A-B)).

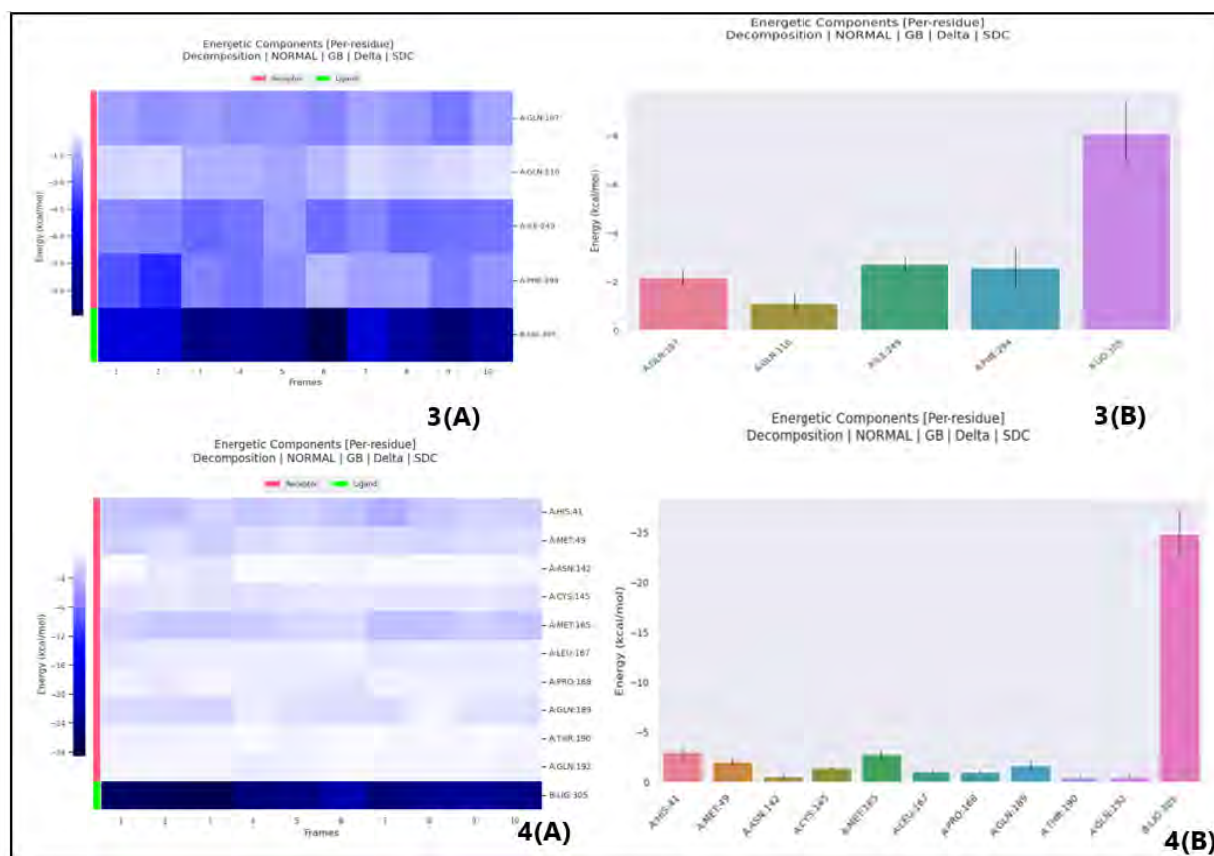


**Fig. 11** (A) Per-residues decomposition result of all two reference compounds (Reference compound 1 **3A-B**), Reference compound 2 **4A-B**).

In our study, Norquinadoline A exhibited the highest negative binding energy at  $-10.0$  kcal/mol, surpassing Reference compound 1 (Baricitinib) at  $-7.5$  kcal/mol and Reference compound 2 (Remdesivir) at  $-8.1$  kcal/mol. Notably, Norquinadoline A outperformed Quinadoline B. It is worth mentioning that Reference compound 2, Remdesivir, is employed in emergencies due to the absence of alternative drugs, despite having a high molecular weight, a greater number of hydrogen bond acceptors, and rotatable bonds, rendering it non-compliant with Lipinski's Rule of Five and outside the range in the BOILED-Egg model.

Reference compound 1 (Baricitinib), an FDA-approved rheumatoid arthritis medication, has demonstrated safety and efficacy in COVID-19 treatment, particularly when used in combination. Our study indicates that mycomolecules, specifically Norquinadoline A and Quinadoline B, outshine phytomolecules as potent inhibitors of the SARS-CoV-2 Mpro. Furthermore, this study also revealed that Norquinadoline A favored over the earlier reported most potential compound such as Quinadoline B (Quimque et al., 2021; Raihan et al., 2021). It is noteworthy that while Baricitinib may show greater stability in MD simulation, our top two compounds demonstrated high docking binding energy, stability in MD simulation, and high binding free energy. Consequently, these two compounds are considered superior mycomolecular inhibitors against SARS-CoV-2's Mpro, emphasizing their potential for further development. Overall, our findings underscore the potential of mycomolecules as superior Mpro inhibitors against SARS-CoV-2.

#### 4 Conclusions

Since emergence of COVID-19, intensive research on bioactive natural compounds, especially on myco-

and phyto-compounds, was carried out towards finding an effective and safe drug against SARS-CoV-2 that resulted several molecules as potential Mproinhibitors of SARS-CoV-2. This study represents the significant strides made in exploring bioactive natural compounds, specifically myco- and phyto-compounds, as potential Mpro inhibitors against SARS-CoV-2 since the onset of the COVID-19 pandemic. By synthesizing dispersed knowledge, we have assembled key inhibitors with proven antiviral activities, offering valuable insights into the current progress of therapeutic approaches involving phytomolecules and mycomolecules. Through systematic in silico screening, we identified top ten compounds, setting the stage for subsequent experimental validation. In-depth molecular dynamics studies and MM/PBSA analysis culminated in the recognition of Norquinadoline A as the most potent Mpro inhibitor of SARS-CoV-2. The promise exhibited by Norquinadoline A positions it as a potential drug lead pending rigorous experimental validations and in-vivo observations. Therefore, the present study provides a valuable advancement in the development of bioactive natural compound-based treatment of COVID-19.

### Acknowledgment

AS thanks Arup Acharjee for useful discussion on fungus-produced compounds.

### References

- Abdelghany TM, Ganash M, Bakri MM, Qanash H, Al-Rajhi AM, Elhussieny NI. 2021. SARS-CoV-2, the other face to SARS-CoV and MERS-CoV: Future predictions. *Biomedical Journal*, 44(1): 86-93. <https://doi.org/10.1016/j.bj.2020.10.008>
- Abraham MJ, Murtola T, Schulz R, Páll S, Smith JC, Hess B, Lindahl E. 2015. GROMACS: High performance molecular simulations through multi-level parallelism from laptops to supercomputers. *SoftwareX*, 1: 19-25. <https://doi.org/10.1016/j.softx.2015.06.001>
- Anton DB, Galvez Bulhões Pedreira J, Zvirtes ML, Laufer SA, Ducati RG, Goettert M, Saraiva Macedo Timmers LF. 2023. Targeting SARS-CoV-2 main protease (MPro) with kinase inhibitors: a promising approach for discovering antiviral and anti-inflammatory molecules against SARS-CoV-2. *Journal of Chemical Information and Modeling*, 63(13): 4138-4146. <https://doi.org/10.1021/acs.jcim.3c00324>
- Banerjee R, Perera L, Tillekeratne LV. 2021. Potential SARS-CoV-2 main protease inhibitors. *Drug Discovery Today*, 26(3): 804-816. <https://doi.org/10.1016/j.drudis.2020.12.005>
- Barlow DJ, Buriani A, Ehrman T, Bosisio E, Eberini I, Hylands PJ. 2012. In-silico studies in Chinese herbal medicines' research: evaluation of in-silico methodologies and phytochemical data sources, and a review of research to date. *Journal of Ethnopharmacology*, 140(3): 526-534. <https://doi.org/10.1016/j.jep.2012.01.041>
- Belachew AM, Feyisa A, Mohamed SB, W/Mariam JF. 2021. Investigating fungi-derived bioactive molecules as inhibitor of the SARS coronavirus papain like protease: computational based study. *Frontiers in Medicine*, 8: 752095. <https://doi.org/10.3389/fmed.2021.752095>
- Bhardwaj VK, Singh R, Das P, Purohit R. 2021. Evaluation of acridinedione analogs as potential SARS-CoV-2 main protease inhibitors and their comparison with repurposed anti-viral drugs. *Computers in Biology and Medicine*, 128: 104117. <https://doi.org/10.1016/j.combiomed.2020.104117>
- Bhardwaj VK, Singh R, Sharma J, Rajendran V, Purohit R, Kumar S. 2021. Identification of bioactive molecules from tea plant as SARS-CoV-2 main protease inhibitors. *Journal of Biomolecular Structure and Dynamics*, 39(10): 3449-3458. <https://doi.org/10.1080/07391102.2020.1766572>
- Bussi G, Donadio D, Parrinello M. 2007. Canonical sampling through velocity rescaling. *The Journal of*

- Chemical Physics, 126(1): 014101. <https://doi.org/10.1063/1.2408420>
- Chen CP, Chen CC, Huang CW, Chang YC. 2018. Evaluating molecular properties involved in transport of small molecules in stratum corneum: A quantitative structure-activity relationship for skin permeability. *Molecules*, 23(4): 911. <https://doi.org/10.3390/molecules23040911>
- Chera A, Tanca A. 2022. Remdesivir: the first FDA-approved anti-COVID-19 Treatment for Young Children. *Discoveries*, 10(2): e151. <https://doi.org/10.15190/d.2022.10>
- Chikhale RV, Sinha SK, Patil RB, Prasad SK, Shakya A, Gurav N, Prasad R, Dhaswadikar SR, Wanjari M, Gurav SS. 2021. In-silico investigation of phytochemicals from *Asparagus racemosus* as plausible antiviral agent in COVID-19. *Journal of Biomolecular Structure and Dynamics*, 39(14): 5033-5047. <https://doi.org/10.1080/07391102.2020.1784289>
- Dai W, Zhang B, Jiang XM, Su H, Li J, Zhao Y, Xie X, Jin Z, Peng J, Liu F, Li C. 2020. Structure-based design of antiviral drug candidates targeting the SARS-CoV-2 main protease. *Science*, 368(6497): 1331-1335. <https://doi.org/10.1126/science.abb4489>
- Daina A, Michielin O, Zoete V. 2017. SwissADME: a free web tool to evaluate pharmacokinetics, drug-likeness and medicinal chemistry friendliness of small molecules. *Scientific Reports*, 7(1): 42717. <https://doi.org/10.1038/srep42717>
- Daina A, Zoete V. 2016. A BOILED-egg to predict gastrointestinal absorption and brain penetration of small molecules. *ChemMedChem*, 11(11), 1117–1121. <https://doi.org/10.1002/cmdc.201600182>
- Darden T, York D, Pedersen L. 1993. Particle mesh Ewald: An  $N \cdot \log(N)$  method for Ewald sums in large systems. *The Journal of Chemical Physics*, 98(12): 10089-10092. <https://doi.org/10.1063/1.464397>
- Douangamath A, Fearon D, Gehrtz P, Krojer T, Lukacik P, Owen CD, Resnick E, Strain-Damerell C, Aimon A, Ábrányi-Balogh P, Brandão-Neto J. 2020. Crystallographic and electrophilic fragment screening of the SARS-CoV-2 main protease. *Nature Communications*, 11(1): 5047. <https://doi.org/10.1038/s41467-020-18709-w>
- Genheden S, Ryde U. 2015. The MM/PBSA and MM/GBSA methods to estimate ligand-binding affinities. *Expert Opinion on Drug Discovery*, 10(5): 449-461. <https://doi.org/10.1517/17460441.2015.1032936>
- Ghosh R, Chakraborty A, Biswas A, Chowdhuri S. 2022. Computer aided identification of potential SARS CoV-2 main protease inhibitors from diterpenoids and biflavonoids of *Torreya nucifera* leaves. *Journal of Biomolecular Structure and Dynamics*, 40(6): 2647-2662. <https://doi.org/10.1080/07391102.2020.1841680>
- Gorbalenya A, Baker S, Baric RS, de Groot R, Drosten C, Gulyaeva AA, Haagmans B, Lauber C, Leontovich AM, Neuman BW, Penzar D. 2020. The species Severe acute respiratory syndrome-related coronavirus: classifying 2019-nCoV and naming it SARS-CoV-2. *Nature Microbiology*, 5(4): 536-544. <https://doi.org/10.1038/s41564-020-0695-z>
- Hess B, Bekker H, Berendsen HJ, Fraaije JG. 1997. LINCS: a linear constraint solver for molecular simulations. *Journal of Computational Chemistry*, 18(12): 1463-1472. [https://doi.org/10.1002/\(SICI\)1096-987X\(199709\)18:12<1463::AID-JCC4>3.0.CO;2-H](https://doi.org/10.1002/(SICI)1096-987X(199709)18:12<1463::AID-JCC4>3.0.CO;2-H)
- Hossain A, Rahman ME, Rahman MS, Nasirujjaman K, Matin MN, Faruqe MO, Rabbee MF. 2023. Identification of medicinal plant-based phytochemicals as a potential inhibitor for SARS-CoV-2 main protease (Mpro) using molecular docking and deep learning methods. *Computers in Biology and Medicine*, 157: 106785. <https://doi.org/10.1016/j.combiomed.2023.106785>
- Hostettmann K, Marston A, Ndjoko K, Wolfender JL. 2000. The potential of African plants as a source of drugs. *Current Organic Chemistry*, 4(10): 973-1010. <https://doi.org/10.2174/1385272003375923>
- Khushboo, Kumari P, Sharma B, Som A. 2024. (2-Cyclohexyl-1-methylpropyl) cyclohexane isolated from

- garlic extract exhibits antidepressant-like activity: extraction, docking, drug-like properties, molecular dynamics simulations and MM/GBSA studies. *Journal of Biomolecular Structure and Dynamics*, 42(4): 1765-1777. <https://doi.org/10.1080/07391102.2023.2202250>
- Kumari P, Pratap Singh S, Som A. 2021. Insights into the dynamics of cyclic diguanosine monophosphate I riboswitch using molecular dynamics simulation. *Indian Journal of Biochemistry and Biophysics (IJBB)*, 58(3): 208-218. <http://op.niscpr.res.in/index.php/IJBB/article/view/37679/0>
- Kumari P, Pradhan B, Koromina M, Patrinos GP, Steen KV. 2022. Discovery of new drug indications for COVID-19: A drug repurposing approach. *Plos One*, 17(5): e0267095. <https://doi.org/10.1371/journal.pone.0267095>
- Lipinski CA. 2004. Lead-and drug-like compounds: the rule-of-five revolution. *Drug Discovery Today: Technologies*, 1(4): 337-341. <https://doi.org/10.1016/j.ddtec.2004.11.007>
- Lu J, Lu W, Jiang H, Yang C, Dong X. 2022. Molecular docking and dynamics of phytochemicals from Chinese herbs with SARS-CoV-2 RdRp. *Natural Product Communications*, 17(6): 1-7. <https://doi.org/10.1177/1934578x221105693>
- Majnooni MB, Fakhri S, Shokohinia Y, Kiyani N, Stage K, Mohammadi P, Gravandi MM, Farzaei MH, Echeverría J. 2020. Phytochemicals: potential therapeutic interventions against coronavirus-associated lung injury. *Frontiers in Pharmacology*, 11: 588467. <https://doi.org/10.3389/fphar.2020.588467>
- Nag A, Banerjee R, Chowdhury RR, Krishnapura Venkatesh C. 2021. Phytochemicals as potential drug candidates for targeting SARS CoV 2 proteins, an in-silico study. *VirusDisease*, 32(1): 98-107. <https://doi.org/10.1007/s13337-021-00654-x>
- Nallusamy S, Mannu J, Ravikumar C, Angamuthu K, Nathan B, Nachimuthu K, Ramasamy G, Muthurajan R, Subbarayalu M, Neelakandan K. 2021. Exploring phytochemicals of traditional medicinal plants exhibiting inhibitory activity against main protease, spike glycoprotein, RNA-dependent RNA polymerase and non-structural proteins of SARS-CoV-2 through virtual screening. *Frontiers in Pharmacology*, 12: 667704. <https://doi.org/10.3389/fphar.2021.667704>
- Ogunyemi OM, Gyebi GA, Elfiky AA, Afolabi SO, Ogunro OB, Adegunloye AP, Ibrahim IM. 2020. Alkaloids and flavonoids from African phytochemicals as potential inhibitors of SARS-Cov-2 RNA-dependent RNA polymerase: an in silico perspective. *Antiviral Chemistry and Chemotherapy*, 28: 1-15. <https://doi.org/10.1177/2040206620984076>
- Parrinello M, Rahman A. 1981. Polymorphic transitions in single crystals: A new molecular dynamics method. *Journal of Applied Physics*, 52(12): 7182-7190. <https://doi.org/10.1063/1.328693>
- Patel CN, Jani SP, Jaiswal DG, Kumar SP, Mangukia N, Parmar RM, Rawal RM, Pandya HA. 2021. Identification of antiviral phytochemicals as a potential SARS-CoV-2 main protease (Mpro) inhibitor using docking and molecular dynamics simulations. *Scientific Reports*, 11(1): 20295. <https://doi.org/10.1038/s41598-021-99165-4>
- Quimque MT, Notarte KI, Fernandez RA, Mendoza MA, Liman RA, Lim JA, Pilapil LA, Ong JK, Pastrana AM, Khan A, Wei DQ. 2021. Virtual screening-driven drug discovery of SARS-CoV2 enzyme inhibitors targeting viral attachment, replication, post-translational modification and host immunity evasion infection mechanisms. *Journal of Biomolecular Structure and Dynamics*, 39(12): 4316-4333. <https://doi.org/10.1080/07391102.2020.1776639>
- Raihan T, Rabbee MF, Roy P, Choudhury S, Baek KH, Azad AK. 2021. Microbial metabolites: the emerging hotspot of antiviral compounds as potential candidates to avert viral pandemic alike COVID-19. *Frontiers in Molecular Biosciences*, 8: 732256. <https://doi.org/10.3389/fmolb.2021.732256>
- Roshni J, Vaishali R, Ganesh KS, Dharani N, Alzahrani KJ, Banjer HJ, Alghamdi AH, Theyab A, Ahmed SS,

- Patil S. 2022. Multi-target potential of Indian phytochemicals against SARS-CoV-2: A docking, molecular dynamics and MM-GBSA approach extended to Omicron B. 1.1. 529. *Journal of Infection and Public Health*, 15(6): 662-669. <https://doi.org/10.1016/j.jiph.2022.05.002>
- Rubin R. 2022. Baricitinib Is First Approved COVID-19 Immunomodulatory Treatment. *JAMA*, 327: 2281. <https://doi.org/10.1001/jama.2022.9846>
- Rubio-Martínez J, Jiménez-Alesanco A, Ceballos-Laita L, Ortega-Alarcón D, Vega S, Calvo C, Benítez C, Abian O, Velázquez-Campoy A, Thomson TM, Granadino-Roldán JM. 2021. Discovery of diverse natural products as inhibitors of SARS-CoV-2 Mpro protease through virtual screening. *Journal of Chemical Information and Modeling*, 61(12): 6094-6106. <https://doi.org/10.1021/acs.jcim.1c00951>
- Shanmugarajan DPP, Kumar BRP, Suresh B. 2020. Curcumin to inhibit binding of spike glycoprotein to ACE2 receptors: computational modelling, simulations, and ADMET studies to explore curcuminoids against novel SARS-CoV-2 targets. *RSC Advances*, 10: 31385–31399. <https://doi.org/10.1039/D0RA03167D>
- Sharma J, Bhardwaj VK, Singh R, Rajendran V, Purohit R, Kumar S. 2021. An in-silico evaluation of different bioactive molecules of tea for their inhibition potency against non structural protein-15 of SARS-CoV-2. *Food Chemistry*, 346: 128933. <https://doi.org/10.1016/j.foodchem.2020.128933>.
- Sharma A, Vora J, Patel D, Sinha S, Jha PC, Shrivastava N. 2022. Identification of natural inhibitors against prime targets of SARS-CoV-2 using molecular docking, molecular dynamics simulation and MM-PBSA approaches. *Journal of Biomolecular Structure and Dynamics*, 40(7): 3296-3311. <https://doi.org/10.1080/07391102.2020.1846624>
- Shitrit A, Zaidman D, Kalid O, Bloch I, Doron D, Yarnizky T, Buch I, Segev I, Ben-Zeev E, Segev E, Kobilier O. 2020. Conserved interactions required for inhibition of the main protease of severe acute respiratory syndrome coronavirus 2 (SARS-CoV-2). *Scientific Reports*, 10(1): 20808. <https://doi.org/10.1038/s41598-020-77794-5>
- Singh R, Bhardwaj VK, Purohit R. 2021. Potential of turmeric-derived compounds against RNA-dependent RNA polymerase of SARS-CoV-2: an in-silico approach. *Computers in Biology and Medicine*, 139: 104965. <https://doi.org/10.1016/j.combiomed.2021.104965>
- Singh R, Bhardwaj VK, Purohit R. 2022. Inhibition of nonstructural protein 15 of SARS-CoV-2 by golden spice: A computational insight. *Cell Biochemistry and Function*, 40(8): 926-934. <https://doi.org/10.1002/cbf.3753>
- Singh R, Bhardwaj VK, Sharma J, Kumar D, Purohit R. 2021. Identification of potential plant bioactive as SARS-CoV-2 Spike protein and human ACE2 fusion inhibitors. *Computers in Biology and Medicine*, 136: 104631. <https://doi.org/10.1016/j.combiomed.2021.104631>
- Singh VK, Chaurasia H, Kumari P, Som A, Mishra R, Srivastava R, Naaz F, Singh A, Singh RK. 2022a. Design, synthesis, and molecular dynamics simulation studies of quinoline derivatives as protease inhibitors against SARS-CoV-2. *Journal of Biomolecular Structure and Dynamics*, 40(21): 10519-10542. <https://doi.org/10.1080/07391102.2021.1946716>
- Singh VK, Chaurasia H, Mishra R, Srivastava R, Yadav AK, Dwivedi J, Singh P, Singh RK. 2022b. COVID-19: pathophysiology, transmission, and drug development for therapeutic treatment and vaccination strategies. *Current Pharmaceutical Design*, 28(27): 2211-2233. <https://doi.org/10.2174/1381612828666220729093340>
- Singh VK, Kumari P, Som A, Rai S, Mishra R, Singh RK. 2023. Design, synthesis and antimicrobial activity of novel quinoline derivatives: an in silico and in vitro study. *Journal of Biomolecular Structure and Dynamics*, 14: 1-21. <https://doi.org/10.1080/07391102.2023.2236716>

- Som A, Sharma AK, Kumari P. 2022. Recombination in sarbecovirus lineage and mutations/insertions in spike protein are linked to the emergence and adaptation of SARS-CoV-2. *Bioinformatics*, 18(10): 951-961. <https://doi.org/10.6026/97320630018951>
- Sriramulu DK, Lee SG. 2021. Effect of molecular properties of the protein-ligand complex on the prediction accuracy of AutoDock. *Journal of Molecular Graphics and Modelling*, 106: 107921. <https://doi.org/10.1016/j.jmgm.2021.107921>
- Swain SS, Panda SK, Luyten W. 2021. Phytochemicals against SARS-CoV as potential drug leads. *Biomedical Journal*, 44(1): 74-85. <https://doi.org/10.1016/j.bj.2020.12.002>
- Tam NM, Pham MQ, Nguyen HT, Hong ND, Hien NK, Quang DT, Phung HT, Ngo ST. 2021. Potential inhibitors for SARS-CoV-2 Mpro from marine compounds. *RSC Advances*, 11(36): 22206-22213. <https://doi.org/10.3389/fmed.2021.752095>
- Turner PJ. 2005. XMGRACE, Version 5.1. 19. Center for Coastal and Land-Margin Research, Oregon Graduate Institute of Science & Technology, USA
- V'kovski P, Kratzel A, Steiner S, Stalder H, Thiel V. 2021. Coronavirus biology and replication: implications for SARS-CoV-2. *Nature Reviews Microbiology*, 19(3): 155-170. <https://doi.org/10.1038/s41579-020-00468-6>
- Vanommeslaeghe K, MacKerell Jr AD. 2015. CHARMM additive and polarizable force fields for biophysics and computer-aided drug design. *Biochimica et Biophysica Acta (BBA)*, 1850(5): 861-871. <https://doi.org/10.1016/j.bbagen.2014.08.004>
- Vilar S, Chakrabarti M, Costanzi S. 2010. Prediction of passive blood–brain partitioning: straightforward and effective classification models based on in silico derived physicochemical descriptors. *Journal of Molecular Graphics and Modelling*, 28(8): 899-903. <https://doi.org/10.1016/j.jmgm.2010.03.010>
- Wang KY, Liu F, Jiang R, Yang X, You T, Liu X, Xiao CQ, Shi Z, Jiang H, Rao Z, Yang H. 2020. Structure of Mpro from COVID-19 virus and discovery of its inhibitors. *Nature*, 582(7811): 289-293. <https://doi.org/10.1101/2020.02.26.964882>
- Yadav R, Chaudhary JK, Jain N, Chaudhary PK, Khanra S, Dhamija P, Sharma A, Kumar A, Handu S. 2021. Role of structural and non-structural proteins and therapeutic targets of SARS-CoV-2 for COVID-19. *Cells*, 10(4): 821. <https://doi.org/10.3390/cells10040821>
- Zoete V, Cuendet MA, Grosdidier A, Michielin O. 2011. SwissParam: a fast force field generation tool for small organic molecules. *Journal of Computational Chemistry*, 32(11): 2359-68. <https://doi.org/10.1002/jcc.21816>